Luminescence Diffusion Tomography

Jenghwa Chang[1], Harry Graber[2], Randall L. Barbour[1,2]
Department of Pathology[1] and Department of Physiology and Biophysics[2], SUNY Health Science Center at Brooklyn, Brooklyn, NY 11203, TEL: 718-270-1286, FAX: 718-270-3313

The excitation light and emission light associated with a luminescence process are governed by a set of coupled time–dependent radiative transfer equations (RTE) [1]. For details of these equations and notations, see accompanying paper [2]. Let R be the reading of a given detector for the emitted intensity, and r_2 be the detector sensitivity function. Then

$$R = \int_V \int_{4\pi} r_2 \otimes \left(\int_{V'} \int_{4\pi} q_2' \otimes G_2(\mathbf{r}, \Omega; \mathbf{r}', \Omega'; t) d\Omega' d^3 r' \right) d\Omega d^3 r = \int_V \frac{\gamma}{4\pi\tau} N_s \otimes \bar{\phi}_2^+ d^3 r, \tag{1}$$

where the $\otimes$ symbol denotes a convolution in time, N_s is the fluorophore/phosphor concentration in the excited state, $q_2 = \frac{\gamma}{4\pi\tau} N_s$ is the equivalent emission source, γ is the quantum yield, τ is the mean lifetime, $G_2(\mathbf{r}, \Omega; \mathbf{r}', \Omega'; t)$ is the Green's function at $\mathbf{r}$ in direction Ω with the source located at $\mathbf{r}'$ in direction Ω', and $\bar{\phi}_2^+ = \int_{4\pi} \int_{V'} \int_{4\pi} r_2' \otimes G_2(\mathbf{r}, -\Omega; \mathbf{r}', -\Omega'; t) d\Omega' d^3 r' d\Omega$. The frequency domain detector readings are obtained by Fourier transforming Eq. (1):

$$\tilde{R} = \int_V \frac{\gamma}{4\pi\tau} \tilde{N}_s \tilde{\bar{\phi}}_2^+ d^3 r, \tag{2}$$

where "~" denotes the Fourier transform. Let N_0 be the total fluorophore/phosphor concentration. Then the Fourier transforms of $\tilde{N}_g$ and $\tilde{N}_s$ are [2]:

$$j\omega\tau \tilde{N}_g = -\frac{\tau \Sigma_{T,1\to 2}}{2\pi} \tilde{\bar{\phi}}_1 \otimes \tilde{N}_g - \tilde{N}_g + 2\pi N_0 \delta(\omega) \quad \text{and} \quad \tilde{N}_s = 2\pi N_0 \delta(\omega) - \tilde{N}_g, \tag{3}$$

where $\bar{\phi}_1 = \bar{\phi}_1(\mathbf{r}, t) = \int_{4\pi} \phi_1 \, d\Omega$ is the intensity [cm^{-2} s^{-1}] of the excitation light. For time–harmonic excitation, that is, $\tilde{\bar{\phi}}_1 = 2\pi\phi_1^0 \left[\delta(\omega) + \eta\delta(\omega - \omega_0) \right]$, where η is the modulation, Eq. (3) can be solved using the following approximations. When the saturation level is not significant, *i.e.*, $N_g \approx N_0$, we have

$$\tilde{N}_g(0) = 2\pi N_0 \left(1 - \tau \Sigma_{T,1\to 2} \phi_1^0 \right) \delta(0), \tag{4}$$

$$\tilde{N}_s(\omega_0) = -\tilde{N}_g(\omega_0) = \frac{2\pi\tau \Sigma_{T,1\to 2} N_0 \phi_1^0 \eta}{1 + j\omega_0 \tau} \delta(0). \tag{5}$$

When the saturation level is more significant, the coupling between DC and the fundamental frequency should be considered but the contribution of higher–order harmonics can be ignored, permitting the following approximations:

$$\tilde{N}_g(0) = \frac{2\left(1 + \tau\Sigma_{T,1\to 2}\phi_1^0\right)^2 + 2(\omega_0\tau)^2}{2\left(1 + \tau\Sigma_{T,1\to 2}\phi_1^0\right)^2 + 2(\omega_0\tau)^2 - \left(\tau\Sigma_{T,1\to 2}\varepsilon\phi_1^0\right)^2} \frac{2\pi N_0}{1 + \tau\Sigma_{T,1\to 2}\phi_1^0} \delta(0), \tag{6}$$

$$\tilde{N}_g(\omega_0) = -\tilde{N}_s(\omega_0) = \frac{-\tau\Sigma_{T,1\to 2}\phi_1^0 \eta \left(1 + \tau\Sigma_{T,1\to 2}\phi_1^0 - j\omega_0\tau\right)}{2\left(1 + \tau\Sigma_{T,1\to 2}\phi_1^0\right)^2 + 2(\omega_0\tau)^2 - \left(\tau\Sigma_{T,1\to 2}\phi_1^0\eta\right)^2} \frac{2\pi N_0}{1 + \tau\Sigma_{T,1\to 2}\phi_1^0} \delta(0). \tag{7}$$

The goal of the inverse problem is to solve equation (2) for $\mu_{T,1\to 2}$, γ, and τ under different source and detection conditions. This requires two reconstruction steps. In the first step, we solve for the background absorption and scattering coefficients, μ_a and μ_s, of the medium for the excitation and the emission photons separately using

previously developed techniques [3]. The second step is to reconstruct $\mu_{T,1\to2}$, γ, and τ using estimates of $\tilde{\tilde{\phi}}_1$ and $\tilde{\tilde{\phi}}_2^+$ calculated from Monte Carlo simulations or other numerical methods using the coefficients obtained from the first step. The following are two proposed methods for this second step.

(A) DC source

If we use DC sources, then equation (2) becomes

$$\tilde{R} = \int_V \frac{\Sigma_{T,1\to2}\tilde{\tilde{\phi}}_1\tilde{\tilde{\phi}}_2^+}{4}(\gamma N_0)d^3r = \int_V w(\gamma N_0)d^3r, \tag{8}$$

where $w \equiv w_{\mathrm{DC}} = \Sigma_{T,1\to2}\tilde{\tilde{\phi}}_1\tilde{\tilde{\phi}}_2^+/4$ is the weight function. If $\Sigma_{\mathrm{T},1\to2}$ is known and $\tilde{\tilde{\phi}}_1$ and $\tilde{\tilde{\phi}}_2^+$ can be precalculated assuming that fluorophore is not present, then the unknown quantity γN_0 can be computed by solving a linear system obtained by discretizing (8). Here, only the product of quantum efficiency and fluorophore concentration is found, and they can not be directly separated.

(B) AC source

If modulated sources are used and γN_0 is solved for by analyzing the DC component of the response as described above and we adopt the approximation in Eq. (5), then equation (2) becomes

$$\tilde{R} = \int_V w\frac{1 - j\omega\tau}{1 + \omega^2\tau^2}d^3r, \tag{9}$$

where $w \equiv w_{\mathrm{AC}} = \gamma\Sigma_{T,1\to2}N_0\phi_1^0\eta\tilde{\tilde{\phi}}_2^+/4$. Equation (9) can be discretized, and the real and imaginary parts of the detector readings give rise to two distinct systems of linear equations, from which $1/(1+\omega^2\tau^2)$ and $-\omega\tau/(1+\omega^2\tau^2)$ can be reconstructed. Because ω is known, τ can also be deduced. If the approximation in Eq. (7) is adopted, we get

$$\tilde{R} = \int_V w\frac{2\left(1+\tau\Sigma_{T,1\to2}\phi_1^0 - j\omega_0\tau\right)}{\left[2\left(1+\tau\Sigma_{T,1\to2}\phi_1^0\right)^2 + 2(\omega_0\tau)^2 - \left(\tau\Sigma_{T,1\to2}\phi_1^0\eta\right)^2\right]\left(1+\tau\Sigma_{T,1\to2}\phi_1^0\right)}d^3r, \tag{10}$$

where w is the same as that in Eq. (9). When $\tau\Sigma_{T,1\to2}\phi_1^0 << 1$, Eq. (10) reduces to Eq. (9).

A preliminary experiment was performed and reconstructed images are reported in this summary. Figure 1A shows the experimental tissue phantoms and Figure 1B illustrates the source and detector configurations. The experiment was performed with two balloons and no added dye in the background. A 0.75W, multi-line (average wavelength ~490 μm) argon laser source was used to irradiate the phantom. A filter blocked excitation light from entering the detector. The detector was a Hamamatsu C3140 CCD camera directed normal to the phantom to collect the emission light. A limited illumination angle was used. The detectors were located at every 30° along the border of the cylinder and the source was positioned every 10° from 90° to 150° counterclockwise relative to the source. The source intensity was recorded for each measurement using a Coherent Labmaster-E. Each measurement was then corrected for the dark current, source intensity, and lens aperture. At least two measurements were taken and averaged to obtain the detector readings for each source-detector pair. In the first experiment, balloons containing different volumes (0.8 and 1.2 mL) of Rhodamine 6G dye at a concentration of ~50 μM were embedded in a 8 cm diameter cylindrical phantom filled with 0.2% Intralipid® (% lipid per unit volume). The same cylindrical phantom was used in the second experiment, but the Intralipid concentration was 0.33% and it contained 0.1 μM dye. The volume of the balloon was 0.5 mL, and contained 100 μM dye.

The optical thickness of the phantom medium was ~20 and ~33 transport mean free pathlengths, respectively, for the excitation and emission light. Weight functions for the corresponding reference media were computed by

Monte Carlo simulations assuming an optical thickness of 20 transport mean free paths. Image reconstructions were performed using three iterative algorithms — POCS, CGD, and SART — with a rescaling technique and positivity constraints [4]. 2-D reconstruction (Figure 2A) were performed by assuming symmetry along the z-axis and the weight function of voxels with the same z-coordinate were summed up to obtain an integrated value. Only the central plane of the reconstruction results are displayed. Figure 2B demonstrates the cylindrical coordinate system, where the ρ- and ϕ- coordinates are shown in the figure and the z-coordinate is normal to the plane of paper. There are 400 voxels in each plane.

Figure 3 shows the reconstruction results using the CGD method after 10, 100, 1,000, and 10,000 iterations. The two balloons are located, and artifacts are present on the boundary. The two inhomogeneities are about the same size but with different intensities, which roughly coincides with the difference in balloon volume. The image quality improves as the number of iterations increases.

Additional results and work in progress include reconstruction of mean lifetime using time-harmonic sources, comparison of reconstruction results using different derived weight functions, and comparison of reconstruction for phantoms with and without added background fluorophores.

1. *Conceptual Basis for Calculations of Absorbed–Dose Distribution*, NCRP Report No. 108, 1991.
2. J. Chang *et al.*, "Fluorophore/Phosphor Emission Contains Higher Harmonics of the Excitation Modulation Frequency," accompanying paper.
3. J. Chang *et al.*, "Imaging diffusive media using time-independent and time-harmonic sources: dependence of image quality on imaging algorithms, target volume, weight matrix, and view angles," vol. SPIE–2389, (San Jose), Feb. 1995.
4. J. Chang *et al.*, "Image reconstruction of dense scattering media from CW sources using constrained CGD and a matrix rescaling technique," vol. SPIE–2389, (San Jose), Feb. 1995.

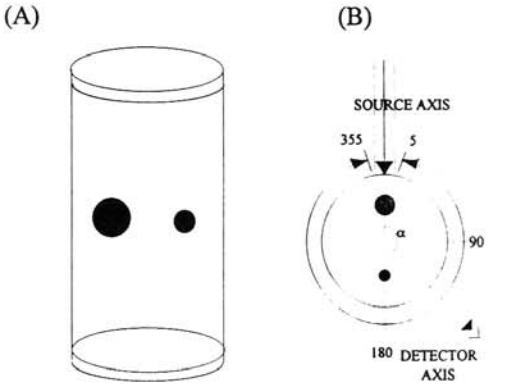

Figure 1. (A) Tissue phantom for the experiment, where two balloons were suspended in the cylinder; (B) Source and detector configurations.

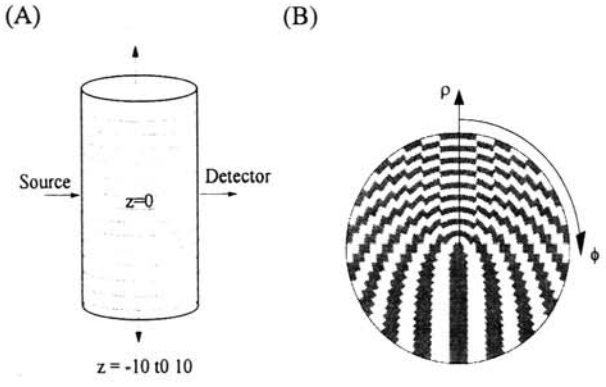

Figure 2. Three reconstruction types – (A) Type-1 reconstruction where axial symmetry was assumed along the z-axis, The cylindrical coordinate system used to discretize the phantom is shown in (D).

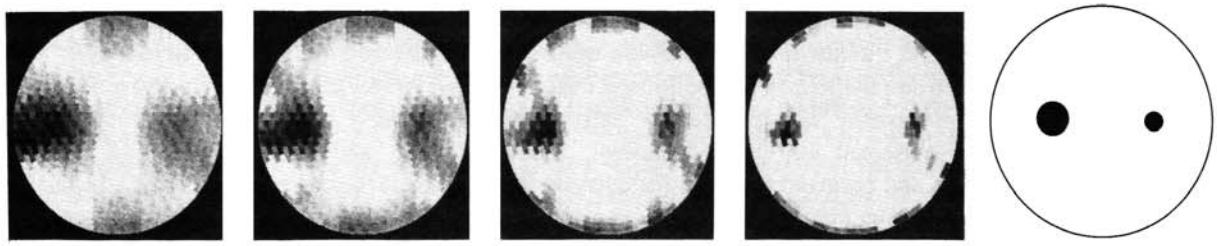

(A) 10 iterations (B) 100 iterations (C) 1,000 iterations (D) 10,000 iterations (E) Target

Figure 3. Type-1 reconstruction results from the first experiment using CGD method after (A) 10 iterations, (B) 100 iterations, (C) 1,000 iterations, and (D) 10,000 iterations. The target is shown in (E).